CLEAVAGE CRACKING RESISTANCE OF HIGH ANGLE GRAIN BOUNDARIES IN *Fe*-3%*Si* ALLOY

A. S. Argon* and Y. Qiao
Department of Mechanical Engineering, Massachusetts Institute of Technology
Cambridge, MA 02139

ABSTRACT

High angle grain boundaries in steel offer an important resistance to the propagation of cleavage cracks that affects the fracture toughness and can modulate the ductile to brittle transition temperature of fracture downward. This behavior has been studied now in bicrystals of *Fe*-3%*Si* alloy in detail. It was noted that the twist misorientation across a high angle boundary has a more profound effect on cleavage fracture resistance than the tilt misorientation. Specific measurements of such resistance at –20°C over a random selection of high angle grain boundaries in bicrystals and associated fractographic studies have led to quantitative models of this resistance. The study has also revealed a transition from pure cleavage to mixed cleavage around 0°C for this alloy above which the observed increment of fracture work could be associated with the sigmoidal plastic bending and rupture of ligaments left between separate primary cleavage strips in the adjoining grain.

Keywords: high angle grain boundaries; cleavage resistance of boundaries; *Fe*-3%*Si* alloy.

1.0 INTRODUCTION

The subject of high angle grain boundaries and their role in affecting the plastic resistance and fracture behavior of polycrystals has been of continued interest. In an early fundamental experimental study of the processes that lead to transitions of fracture from ductile to brittle forms in polycrystalline steel, Hahn, et al. (1959) noted that with decreasing temperature and rapidly increasing plastic resistance, prior to the onset of full brittleness, slip induced dormant, grain-sized, microcracks appear. This indicated that grain boundaries offer an important resistance to the propagation of cleavage cracks in the nature of acting as "fire breaks". It is this particular role of high angle grain boundaries in affecting cleavage cracking resistance that is of primary interest here. While this behavior has been well appreciated, definitive studies of it are rare. The few existing studies have been limited to the assessment of such resistance by individual grain boundaries with known lattice misorientation in hydrogen charged *Fe*-3%*Si* alloy by Gell and Smith (1967), and to some models considering such resistance by Anderson, et al (1994), by Crocker, et al. (1996) and by McClintock (1997).

In the present study we have explored in considerable detail the particular forms of break-through of cleavage cracks across specific grain boundaries with known tilt and twist misorientation. The full details of the study are being reported elsewhere (Qiao and Argon, 2002a). Here we provide only a summary of the essential findings.

* Author for correspondence; e-mail: *argon@mit.edu*; Fax: (617)253-2217

2.0 EXPERIMENTAL DETAILS

2.1 Material

The present study using pedigreed bicrystals became possible through the donation of a large ingot of *Fe*-3%*Si* alloy by the Allegheny Ludlum Steel Co. In the slowly cooled ingot of about 12cm thickness the size of grains ranged from roughly 5mm diameter on the outside to about 50-80mm in the interior. The chemical composition of the material by weight percent consisted of 0.63C, 3.4Si with P and S being less than 0.1 and the balance being Fe. Metallographic examination of the as-received ingot revealed a large concentration of very substantial size elongated carbides and a high concentration of ubiquitous narrow deformation twins, in most of the possible variant directions. The carbides were removed by a special two-step schedule of decarburization that is described in detail elsewhere (Qiao and Argon, 2002a). After decarburization the carbon content decreased to 0.06% and was entirely in solution.

2.2 Material Preparation

2.2.1 Extraction of bicrystals from the ingot

The entire set of bicrystals used in this investigation were extracted from a 6mm thick slice taken from the *Fe*-3%*Si* alloy ingot. The slice was surface ground to a fine finish and etched for approximately 10 hours in a 3% *nital* etch to reveal the low energy (100) cleavage facets in the large collection of grains contained in the slice. Using a special optical scanning procedure of the reflections of light from the (100) etching facets it was possible to determine quite effectively those large grains that had (100) planes parallel to the ground surface, and thus contained a pair of mutually perpendicular cleavage planes normal to the ground surface. X-ray Laue back reflection analysis confirmed the accuracy of the crystal orientation. These large grains, identified as *A*, with their adjoining family of attached grains became candidates for extraction as bicrystals by electrical discharge machining (Qiao and Argon, 2002a). The orientation of the surrounding *B* grains to be used in separate bicrystals were all obtained by X-ray Laue back reflection analysis.

2.2.2 Characterization of lattice misorientations of surrounding grains

As will become clear from our experimental results to be presented in Section 3, the form of interaction of a cleavage crack plane with a grain boundary is governed primarily by the tilt and twist orientations of the adjoining grain across the grain boundary. The angles of tilt ψ, and twist φ of grain *B* across the grain boundary plane, relative to grain *A* can be given as (Qiao and Argon, 2002a)

$$\psi = \frac{\pi}{2} - \cos^{-1}\alpha_{32} \tag{1a}$$

$$\varphi = \frac{\pi}{2} - \cos^{-1}\alpha_{31} \tag{1b}$$

where α_{31} and α_{32} are the direction cosines locating the unit normal vector of the principal cleavage plane of grain *B* relative to the principal axes of grain *A*, parallel to its [100] and [010] directions respectively. Through the form of preparation described below, 17 different bicrystal pairs with relatively random distribution of tilt and twist

angles ψ and φ became available. The characteristics of these bicrystals are given in Table I.

2.2.3 Welding of bicrystals into double cantilever beam "carrier" samples

The average size of the extracted and decarburized bicrystal slabs was 40×10×4mm. These were electron-beam welded into fine grain 1020 steel carriers according to a special welding procedure to minimize residual stresses in the production of the double cantilever beam (DCB) specimens. After welding, the DCB specimens were stress-relieved at 400^{o}C for 3 hours, and subsequently surface ground to a final thickness of somewhat under 4.0mm, and were provided with shallow side grooves of 60^{o} angle with a 45^{o} chevron at the tip of the initial crack. Figure 1 depicts the DCB samples used in the experiments to probe the grain boundary.

2.3 Single Crystal Tension Tests

Single crystal tension specimens were cut out from a single large grain to carry out stress-strain experiments to determine the temperature dependence of the plastic resistance and fracture behavior of the material of interest. The Schmid factor of the principal {110}<111> type slip system was 0.44 while that for the alternative {112}<111> type system was 0.37. Because of the low temperature in the test and the higher Schmid factor, the {110}<111> system was taken to be the active one in the evaluation of the plastic glide resistance.

2.4 The Wedge-loading Test Configuration

To achieve the best conditions of propagating the cleavage cracks to probe the grain boundary in bicrystals in the most stable manner, a stiff wedge-loading arrangement having a minimal compliance C_m was devised. The measured overall compliance C_m of the loading system was 9.0×10^{-8}m/N, which was roughly 1% of the opening compliance of a typical DCB specimen. A simple environment chamber was constructed to control the test temperature through flow of cold nitrogen gas fed into the chamber. Temperature uniformity in the specimen was reached typically within 15 minutes.

3.0 EXPERIMENTAL RESULTS

3.1 Single Crystal Experiments

The temperature dependence of the tensile yield stress, the fracture stress and the critical resolved shear stress (CRSS) on the primary {110}<111> system and the alternative {112}<111> system is given in Fig.2. The rise of the CRSS below 50^{o}C is attributed to a combination of lattice resistance and solid solution resistance arising from *Si*. The scatter in the yield stress in the low-temperature region arises form profusion of twining where the dotted line can be considered as a twining-related yield stress.

3.2 Bicrystal Fracture Experiments at –20^{o}C

Figure 3 shows a result of a typical experiment of the dependence of the DCB opening force P on the associated crack opening displacement δ at the contact point of the wedge. Because the crack tip was usually imperfect as produced, the crack propagation was not of a quasi-static nature. In the figure the solid contour represents the recorded

experimental data while the dashed curve represents an ideal quasi-static reference response. During the load rise from 0-1 the macrocrack with length a_0 (=a_1), as depicted in Fig.1, is flexed, exerting an increasing stress intensity at the tip of the crack across the median cleavage plane of grain *A*. Because of crack tip imperfections the crack becomes overstressed to reach a K_I level exceeding somewhat the K_{IC} for quasi-static growth. At point 1, K_I for initiation of crack growth is reached, the somewhat overstressed crack jumps in an unrestrained manner across grain *A* to come to rest at the grain boundary, and begins to penetrate partially into grain *B*, but a full penetration requires an increase in the crack driving force K_I along a new loading line with smaller slope due to the increased compliance. When point 3 is reached, under the increment ΔK_I, the crack breaks through the grain boundary and penetrates into grain *B* by a further unstable jump, to come to rest on the opposite border of grain *B* with the polycrystalline background, i.e. at point 4. The subsequent serrated loading behavior past point 4 conveys little relevant information.The curve of Fig.3 shows that some frictional effects are present between the wedge and the contacting faces in the DCB specimen even after the application of lubricant, demonstrated by the fact that the loading does not start from zero but from a finite resistance. This artifact is formally rectified by shifting the origin of the loading curves to zero.

From basic beam theory the stress intensity probing the crack tip in grain *A* can be stated as

$$K_I = \Gamma P a_1 \tag{2}$$

where

$$\Gamma = \sqrt{\frac{12}{(1-\nu^2) b b_n h^3}} \tag{2a}$$

in which *P* is the applied DCB opening load with an initial crack length of a_1, *b* is the specimen thickness, b_n the thickness across the root of the side grooves and *h* is the arm height of the DCB sample with ν being the Poisson's ratio. Thus, the initial crack growth resistance K_{ICA} for grain *A* is

$$K_{ICA} = \Gamma P_1 a_1 \tag{3}$$

where a_1 is the initial crack length and P_1 the critical load to initiate its extension at point 1 in Fig.3. Finally, the stress intensity K_{I3} to break through the grain boundary can be taken similarly as

$$K_{I3} = \Gamma P_3 a_2 \tag{4}$$

where a_2 is the total length of the crack abutting on the grain boundary. Then, the incremental fracture toughness ΔK_{ICGB} attributable to the grain boundary fracture resistance is

$$\Delta K_{ICGB} = \Gamma a_2 (P_3 - P_2) . \tag{5}$$

In this manner altogether 17 bicrystal samples with different lattice misorientation between grain *B* and grain *A* were probed. The resulting measurements of the ΔK_{ICGB} for these 17 bicrystal experiments are given in Table I normalized with K_{ICA} and as a function of the individual tilt and twist angles ψ and φ. The measured fracture toughnesses of grains *A* are quite reproducible at an overall level of $\boldsymbol{K}_{ICA} = 14.1 \pm 0.6\, MPa\sqrt{m}$. This relatively high fracture toughness needs some explanation that we will furnish below.

3.3 Fracture Transition Experiments in Bicrystals

To explore how the grain boundary modulates the cleavage cracking across it with changing temperature two sets of additional bicrystal samples were prepared for use in wedge cracking experiments in a temperature range between –20°C to 22°C. In the first set labeled as "C" (Sample 6 in Table I) six other available bicrystal samples identified as sample 6 in Table I, with tilt and twist angles of ψ=7°; φ=42° were used. For the second set labeled as "D" nine bicrystals of a rather different misorientation consisting of ψ=8° φ=12° was extracted from the remaining large slice of the same ingot. The measured ΔK_{ICGB} values normalized with K_{ICA} for these two specimen sets are shown in Fig.4. over the temperature range. The figure shows that there is a readily recognizable transition in the grain boundary cracking resistance between –2°C and 0°C in these two sets, with values for set "C" being distinctly higher. Since the fracture appearance in the entire temperature range remained to be substantially of a cleavage nature, the transition has been labeled as a *cleavage-to-mixed-cleavage transition*. The source of the additional fracture work above the transition temperature is clarified below in Section 3.4.3.

3.4 Fractographic Observations

3.4.1 Fracture surfaces in grain A

Figure 5 shows portions of the cleavage fracture surfaces of grain *A* (in a sample that was not decarburized) at –20°C. A significant interaction of the cleavage crack with the deformation twins is discernable. There are many examples of repeated arrest of the cleavage crack by the narrow twins followed by points of break-through marked by river markings emanating from these points. Stereoscopic SEM observations of the encounters of the crack with twins indicated that the repeated arrest and reinitiation events of the cleavage crack by the twins, fragments the crack plane into separated strips advancing at different levels. Since the fracture toughness in cleavage-like fracture processes correlates well with the fracture surface roughness, this roughness was measured with a Zygo Interferometer* on several fracture surfaces of grain *A* in the low temperature range and was found to be of a rms roughness amplitude of 2.7μm.

3.4.2 Fracture across grain boundaries at –20°C

Fractographic examination of the penetration of the cleavage crack from grain *A* across the boundary into grain *B* exhibited two limiting modes, with most of the penetrations being of a mixed nature. Figure 6a is a micrograph of a "regular mode" of entry of the cleavage crack from grain *A* to grain *B* in bicrystal 14 with similar twist and tilt misorientation (ψ=26°, φ=21°). After initial arrest, and within the characteristic increment of crack tip driving force, as depicted in Fig.3, the arrested cleavage crack front penetrates into grain *B* at a number of relatively evenly spaced points an average distance *w* apart, in the form of a series of "stair-case-like" tiers with flat surfaces of the twist inclination of the planes relative to the cleavage crack plane in grain *A*. In a transition region the individual cleavage facets bow into the designated strips as depicted in the sketch of Fig.6b, forming the tiered cleavage facets of grain *B*. The primary cleavage

* An instrument that uses scanning white light interferometry to image and measure the micro structure and topography of surfaces in three dimensions (New View System 5000 produced by Zygo Corp. of Middlefield, Connecticut).

facets in grain *B* that undercut each other to some extent are bridged by secondary cleavage cracking to complete the stair-case type propagation of cleavage into grain *B*.

Since the distances *w* between the break-through points along a grain boundary were judged to be an important dimension in assessing the penetration resistance of a grain boundary, the number distribution of *w* was measured for several grain boundaries. An example of this distribution in bicrystal 14 is shown in Fig.7. All such measured distributions of *w* showed similar shapes that fitted reasonably well to a lognormal distribution function, with a most probable value in the range of roughly 2.5-3.0μm and quite independent of the twist misorientation. While the origin of this characteristic dimension is unclear, it is likely to be governed by some grain boundary structure and the dynamic nature of the probing. In some other cases, the form of penetration of the cleavage crack across the grain boundary was more irregular than that shown in Fig.6.

3.4.3 Fractures across grain boundaries above the cleavage to mixed-cleavage transition
Fractographic observations of cleavage transition from grain *A* to grain *B* above the 0^{o}C transition temperature indicated very similar features with, however, a significant difference in the appearance of the cleavage fracture surface of grain *B*. The cleavage facets in grain *B* are apparently produced in a very similar manner as depicted in the sketch of Fig.6b. However, instead of the easy formation of secondary cleavage processes bridging the primary facets, the ligaments between facets have undergone considerable sigmoidal plastic bending, shown in Fig.8a and as depicted in the sketch of Fig.8b. This suggests that a significant portion of the additional fracture work in the mixed cleavage plateau occurs not in the initial penetration of the grain boundary but immediately *subsequent* to it, affecting the fracture work of grain *B* all along its length, but requiring a substantial initial increase in the rate of production of fracture work.

4.0 MODELS

4.1 Work of Cleavage in a Grain

As indicated in Table I, the measured fracture toughness K_{ICA} of 14.1MPa$\sqrt{m}$ of individual grains *A* of the bicrystal pairs at -20^{o}C converts to a very substantial work of fracture of G_{ICA} of 850 J/m^2. This very high fracture energy requires explanation. Examination of the fracture surfaces shown in Fig.5 shows only characteristic cleavage markings, but also much evidence of strong interactions of cleavage cracks with deformation twin bands as already noted above, producing fragmentation of the plane of the cleavage crack into separate strips, at somewhat different levels. The net effect of these crack plane shunting processes has been a tiered fracture surface with an rms roughness of 2.7μm as reported above. We view this fragmentation of the crack plane as the source of the crack opening displacement δ_c associated with the crack advance. These fracture surface features are not satisfactorily explained by conventional interpretations of excess fracture work where this work is considered expanded before crack advance. We view the events of crack advance in a different order.

We start by noting that the *Fe*-3%*Si* alloy is an intrinsically brittle solid, embrittled further by the large concentration of *Si* which is a potent solid solution strengthening

agent in *Fe*. When a "steady state" form of crack advance is established, with all of its jerky features, as evidenced from the fracture surface markings of Fig.5 as already noted, the average crack plane becomes fragmented into a set of cleavage strips of average width w_c, and dispersed randomly in height by roughly 2.7μm. This form of the crack topography sets the scale of the work of fracture.

In our view, illustrated in Fig.9a, the cleavage strips of average width w_c penetrate into undeformed material at the tip of a process zone (PZT), of extent Δ_c, without any accompanying plastic dissipation at their tips. This is in conformity with expectations from an intrinsically brittle solid, well below its transition temperature (at 250°C as determined by us, Qiao and Argon, 2002b). As the cleavage strips of the process zone tip advance on planes randomly separated in height over a range of δ_c, the edges of the strips that are left behind undergo secondary cleavage, plastic rubbering and some fragmentation. The major element of dissipative work is then done in the process zone of extent Δ_c, until the two rough crack flanks are separated by the distance δ_c and all contact is terminated at point, CT, of the crack tip. Such a process in which the inelastic dissipation is *subsequent* to the advancement of the cracking front resembles those cases frequently encountered in brittle composites reinforced with discrete fibers of a given length (δ_c) (Argon, 2000). The mechanism of the advance of such a process zone in which a characteristic traction-separation process, illustrated in Fig.9b, "processes" unbroken solid into fully separated crack flanks has been considered in detail by Andersson and Bergkvist (1970). We adopt the findings of their model to our phenomenon. In the Anderson and Bergkvist model which approximates the descending portion of the traction-separation process relation by a straight line over the separation distance CCOD = δ_c, the critical zone size Δ_c is given by:

$$\Delta_c = \beta_c \frac{E}{\sigma_B}(CCOD) \tag{6}$$

where the constant β_c = 0.43 is obtained from a numerical simulation, and σ_B is the average cohesive strength that needs to be overcome to advance the cleavage front forward, and CCOD is taken as the rms roughness range $\delta_c = 2.7\times10^{-6}$m as reported above. With the prevailing parameters given above and σ_B taken as 1.0 GPa, the process zone size is estimated to be 2.5×10^{-4}m. Moreover, the Anderson and Bergkvist development gives the essential work of fracture consisting of the inelastic dissipation process in the process zone as

$$G_{ICA} = \frac{\sigma_B \cdot CCOD}{2} \tag{7}$$

For the above chosen parameters G_{ICA} is 1,350J/m^2, and somewhat larger than the measured value of 850J/m^2, with the discrepancy being readily accountable by the drooping shape of the actual traction-separation relation, differing from that given in Fig.9b.

4.2 Cleavage Resistance of Grain Boundaries

We refer to Fig.6a, representing the regular mode of penetration of the crack across the grain boundary, and to the sketch of Fig.6b. By a quasi-regular sampling process, the

nature of which is not fully clear, the cleavage crack from grain *A* penetrates into grain *B* at points, on the average, a distance *w* apart on the cleavage surface of grain *A* along the outline of the boundary and spreads out on the cleavage terraces in grain *B*, separated by distances $w\sin\varphi$, much like in a crack trapping model of a brittle crack going through tough heterogeneities (Bower and Ortiz, 1991; Mower and Argon, 1995) where the, as yet to be sheared, triangular grain boundary segments are acting momentarily as the heterogeneities. Upon the penetration of the fragmented cleavage terraces into grain *B* by increasing distances Δx (as projected to the extension of the cleavage plane of grain *A*), at a critical Δx_c the opening displacements of the cleavage terraces force apart the remaining triangular grain boundary islands by a combination of cleavage and grain boundary shear over a relative displacement $\delta_B = \beta\Delta x/\cos\psi$. The remaining triangular grain boundary islands finally give-way suddenly when $\delta_B \to \delta_{Bc}$ and Δx reaches a critical level Δx_c, where the maximum grain boundary resistance is reached.

The increase in the expanded energy ΔU required to overcome the boundary resistance is then, made up of two contributions: an increase in exposed cleavage surface ΔA along the terraces of width $w\cos\varphi$, with associated bridging secondary cleavage processes connecting the terraces of height $w\sin\varphi$; and the grain boundary shear work ΔW_p, expanded over the relative grain boundary displacement δ_{Bc}. This gives

$$\Delta U = G_{ICA}\Delta A + \Delta W_p \tag{8}$$

where

$$\Delta A = \Delta x \frac{w}{\cos^2\psi}\left[\sin\varphi + \cos\varphi\right] \tag{9}$$

is the increase of cleavage surface with each penetration distance Δx of the crack into grain *B* (both as projected back on the extension of the cleavage plane of grain *A*), and the tilt angle ψ and twist angle φ accounting for the geometrical projection effects of the actual cleavage areas onto the mean crack advance plane coincident with the extension of the cleavage plane of grain *A*. In Eqn(8) we have assumed that the actual specific work of separation across cleavage areas has remained to be G_{ICA}, the specific fracture work across grain *A*. The work of separation of grain boundary islands, forced apart by the crack penetrating into grain *B*, can be given as

$$\Delta W_p = \frac{\beta w^2 \Delta x}{4} k \frac{\sin\varphi\cos\varphi}{\cos\psi} \tag{10}$$

where *k* is the grain boundary plastic shear resistance. At the point of maximum resistance of the boundary, when Δx reaches Δx_c and δ_B reaches $\delta_{Bc} = \beta\Delta x_c$, the increment of expanded energy will reach its peak value as:

$$\Delta U = G_{ICA} w\Delta x_c \frac{1}{\cos^2\psi}\left(\sin\varphi + \cos\varphi\right) + \beta\frac{kw^2\Delta x_c}{4}\frac{\sin\varphi\cos\varphi}{\cos\psi}, \tag{11}$$

and the overall specific peak grain boundary break-through resistance becomes

$$G_{ICGB} = \frac{\Delta U}{w\Delta x_c} = G_{ICA}\frac{1}{\cos^2\psi}\left(\sin\varphi + \cos\varphi\right) + \frac{\beta k w}{4}\frac{\sin\varphi\cos\varphi}{\cos\psi}, \tag{12}$$

giving the peak stress intensity to break-through the grain boundary as:

$$K_{\mathrm{ICGB}} = \sqrt{\frac{EG_{\mathrm{ICGB}}}{1-\nu^2}}\,. \tag{13}$$

Beyond the peak resistance the second term in Eqn(12) is no longer present and G_{ICB} the resistance of the grain *B* consists of only the first term on the RHS of Eqn(12). Finally, the differential cracking resistance of a grain boundary, normalized with K_{ICA}, becomes simply,

$$\frac{\Delta K_{\mathrm{ICGB}}}{K_{\mathrm{ICA}}} = \sqrt{\frac{1}{\cos^2\psi}\left(\sin\varphi + \cos\varphi\right) + C\frac{\sin\varphi\cos\varphi}{\cos\psi}} - 1 \tag{14}$$

where the constant

$$C = \frac{\beta k w}{4G_{\mathrm{ICA}}} \tag{15}$$

is a material constant combining together both well known and ill-defined factors. The remainder of Eqn(15) is of a purely geometrical nature. We note that for ψ and φ going to zero the grain boundary resistance as given by Eqn(15) vanishes as it should.We consider the parameter *C* as adjustable. To obtain the best fit between the model and the experimental measurements for the 17 different bicrystal experiments, we use experiment 13 with a contribution of substantial tilt and twist to fix *C* as 0.25. With this single fitting constant we have calculated the predictions of Eqn(14) for all 17 cases and compared the model prediction with the experimental measurements. The results represented as a ratio $(\Delta K_{\mathrm{ICGB}})_{\mathrm{E}}/(\Delta K_{\mathrm{ICGB}})_{\mathrm{C}}$ of the experimental measurements to the computed values are given in Table I. While there is some scatter with the largest departure being about 13%, the overall average ratio was found to be:

$$(\Delta K_{\mathrm{ICGB}})_{\mathrm{E}}/(\Delta K_{\mathrm{ICGB}})_{\mathrm{C}} = 1.00 \pm 0.05 \tag{16}$$

which we consider this to be quite good.

Pursuing the model further we consider Eqn(14) also as a framework to calculate the boundary penetration resistance above the cleavage to mixed-cleavage transition where considerable additional dissipative work is being done in the sigmoidal plastic bending of the ligaments connecting the individual cleavage strips in grain *B*. We consider this additional work formally associated with the grain boundary shear work ΔW_{p} of Eqn(10). This is possible by a reinterpretation of the nondimentional constant *C* in Eqns(14) and (15). A new choice of *C* at a level of 1.70 then also successfully accounts for the considerably larger break-through toughness in the two orientations “C” and “D” shown in Fig.4.

Clearly, these fitting exercises demonstrate only a proper framework for considering relative ordering of the measured parameters and does not constitute a fully accurate model.

5.0 DISCUSSION

In the present bicrystal experiments we have demonstrated that the transit of cleavage cracks across grain boundaries is a topologically relatively simple process in the range well below the usual ductile-to-brittle fracture transition in *Fe*-3%*Si* alloy. The latter

transition in polycrystalline samples of this material occurs at a temperature around 250°C (Qiao and Argon, 2002a). Thus, at –20°C, where most of the bicrystal experiments were performed the alloy under consideration is very brittle and the specific role of grain boundaries becomes relatively easily understandable. In our experiments we have found that the work of fracture (critical energy release rate) G_{ICA} of the well aligned grain *A* was in the range of 850J/m^2 which is quite substantial. This high level was accounted for by a model that attributes the high plastic dissipation to the plastic "rubbing" of rough crack flanks as they are being separated. A relatively simple geometrical model guided by relevant SEM fractographs has resulted in a successful framework to account for the break-through resistance of grain boundaries. How these considerations apply to the accounting of the cleavage fracture resistance in polycrystals in the lower-shelf region is the subject for a separate communication (Qiao and Argon, 2002b).

Table I Characteristics of the 17 bicrystal samples: measured values of K_{ICGB}/K_{ICA} and normalized experimental and computed toughness compared

Sample	1	2	3	4	5	6	7	8
ψ	0.175	0.210	0.331	0.157	0.140	0.122	0.140	0.594
φ	0.559	0.052	0.245	0.367	0.332	0.734	0.069	0.210
K_{ICGB}/K_{ICA}	1.461	1.049	1.168	1.226	1.192	1.575	1.042	1.233
$(\Delta K_{ICGB})_E/(\Delta K_{ICGB})_C$	1.132	0.942	0.977	0.967	1.046	1.096	0.964	0.984
Sample	9	10	11	12	13	14	15	16
ψ	0.229	0.402	0.052	0.385	0.210	0.367	0.490	0.524
φ	0.455	0.699	0.052	0.297	0.227	0.455	0.245	0.069
K_{ICGB}/K_{ICA}	1.283	1.602	1.036	1.225	1.141	1.404	1.204	1.121
$(\Delta K_{ICGB})_E/(\Delta K_{ICGB})_C$	1.030	0.923	1.002	0.995	1.000	1.078	0.969	0.921
Sample	17							
ψ	0.280							
φ	0.542							
K_{ICGB}/K_{ICA}	1.425							
$(\Delta K_{ICGB})_E/(\Delta K_{ICGB})_C$	1.073							

ACKNOWLEDGEMENT

This research has been supported at its inception by the Material Science Division of the ONR under Grant N00014-96-1-0629 for which we are grateful to Dr. George Yoder. The research has been supported more recently by the NSF under Grant DMR-9906613. We also gratefully acknowledge receipt of two large blocks of Fe-3%Si ingots from Allegheny Ludlum Steel Co., which made the bicrystal research possible. For this we are particularly grateful to Dr. James A. Salsgiver of the AL Technical Center.

References

Anderson, T. L., Stienstra, D., Dodds Jr., R. H., (1994), in "*Fracture Mechanics: Twenty-Fourth Volume*", edited by Landes, J. D., McCake, D. E. and Boulet, J. A. M., ASTM STP-1207, ASTM: Philadelphia, PA, p.186

Andersson, H. and Bergkvist, H., (1970), *J. Mech. Phys Solids*,**18**, 1.

Argon, A. S., (2000), in "*Comprehensive Composite Materials*", edited by Kelly, A. and Zweben, C., vol. 1 (edited by Chou, T.-W.), Pergamon/Elsevier: Amsterdam, p.763.

Bower, A. F. and Ortiz, M., (1991), *J. Mech. Phys. Solids*, **39**, 815.

Crocker, A., Smith, G., Flewitt, P. and Moskovic, R., (1996), in "Proceedings of the 11th European Conference on Fracture (ECF11)", Eng. Mater. Advis. Serv., Warley, UK, vol.1, pp233-6.

Gell, M. and Smith, E., (1967), *Acta Metall*., **15**, 253.

Hahn, G. T., Averbach, B. L., Owen, W. S., and Cohen, M., (1959), in "*Fracture*", edited by Averbach, B. L., Felbeck, D. K., Hahn, G. T. and Thomas, D. A., MIT Press: Cambridge, MA, p.91.

McClintock, F. A., (1997), in "*Cleavage Fracture: George R. Irwin Symposium Proceedings*", edited by Chan, K. S., TMS: Warrendale, PA, p.81.

Mower, T. M. and Argon, A. S., (1995), *Mech. Mater*., **19**, 343.

Qiao, Y. and Argon, A. S., (2002a), *Mech. Mater*., submitted for publication.

Qiao, Y. and Argon, A. S., (2002b), to be published.

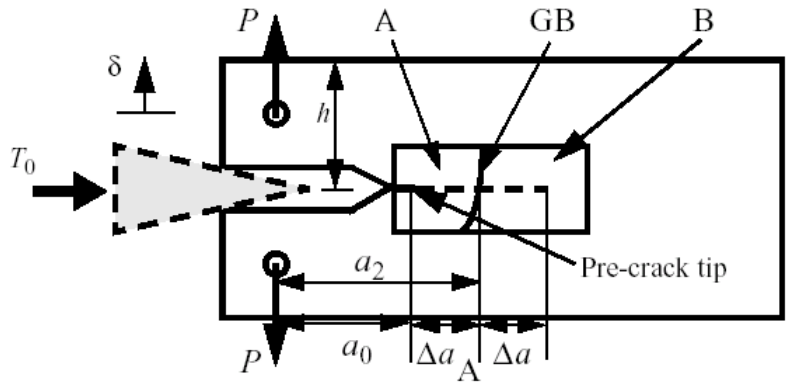

Fig.1 Sketch of double cantilever beam specimen showing the electron-beam welded bicrystal insert (grains *A* and *B*) and means of wedge loading by T_0 to producing opening loads *P*.

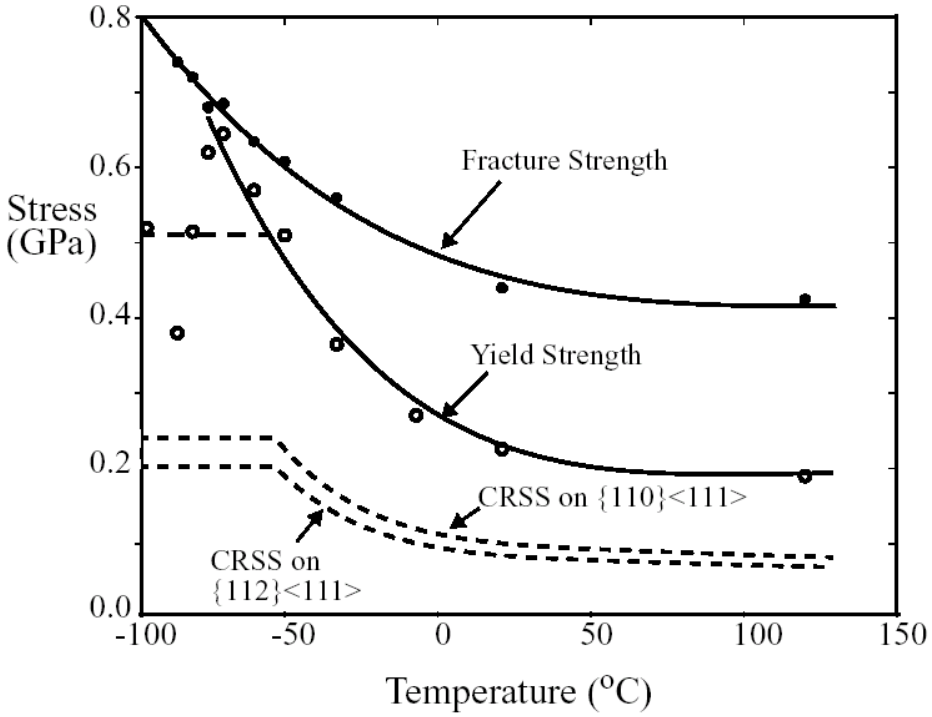

Fig.2 The temperature dependence of the tensile yield stress, fracture stress and critical resolved shear stresses on the possible {110}<111> and {112}<111> slip systems of single crystal experiments.

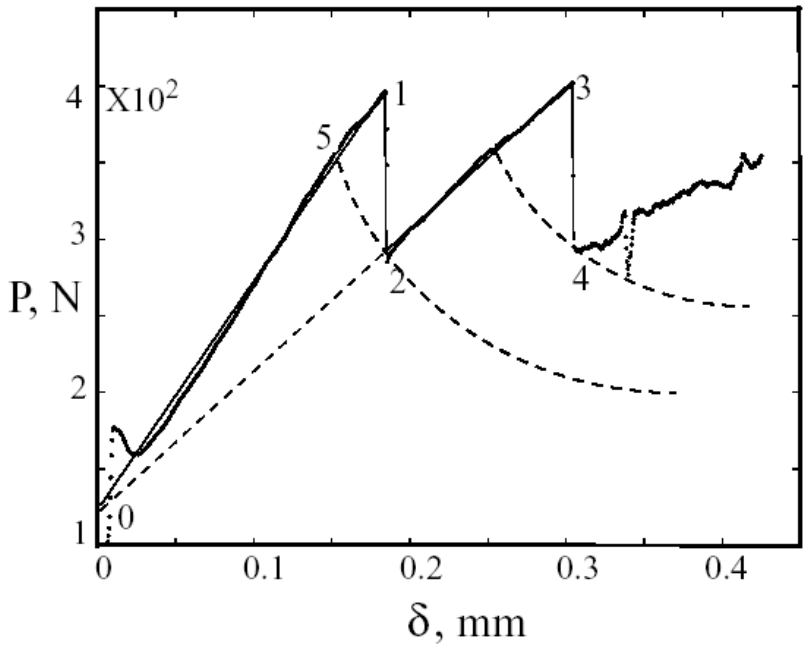

Fig.3 A typical example of the dependence of opening load P on opening displacement δ in a wedge loading experiment (Sample 6).

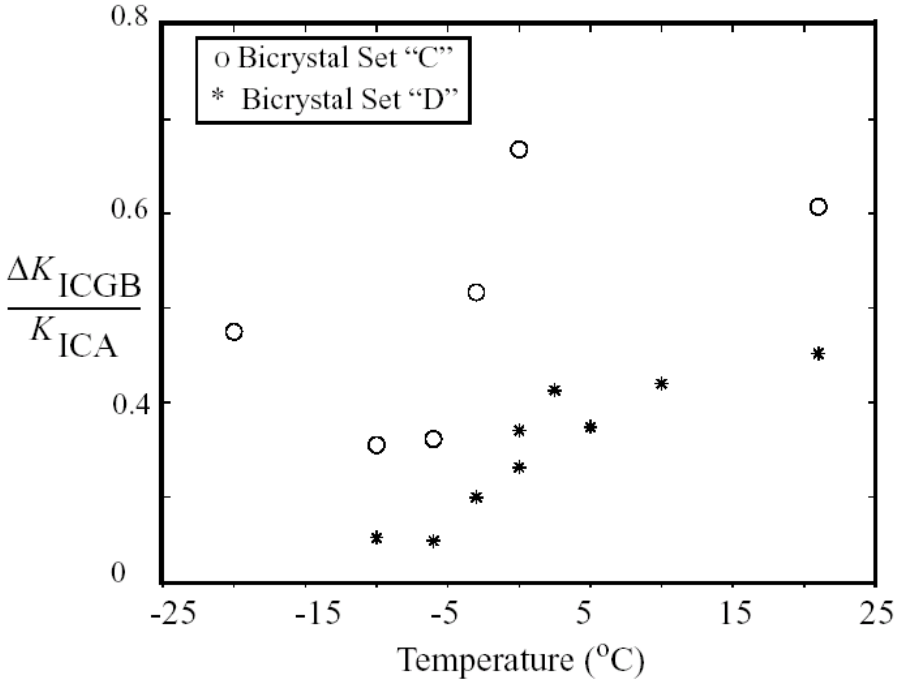

Fig. 4 Transition in the normalized fracture resistance from cleavage to mixed-cleavage.

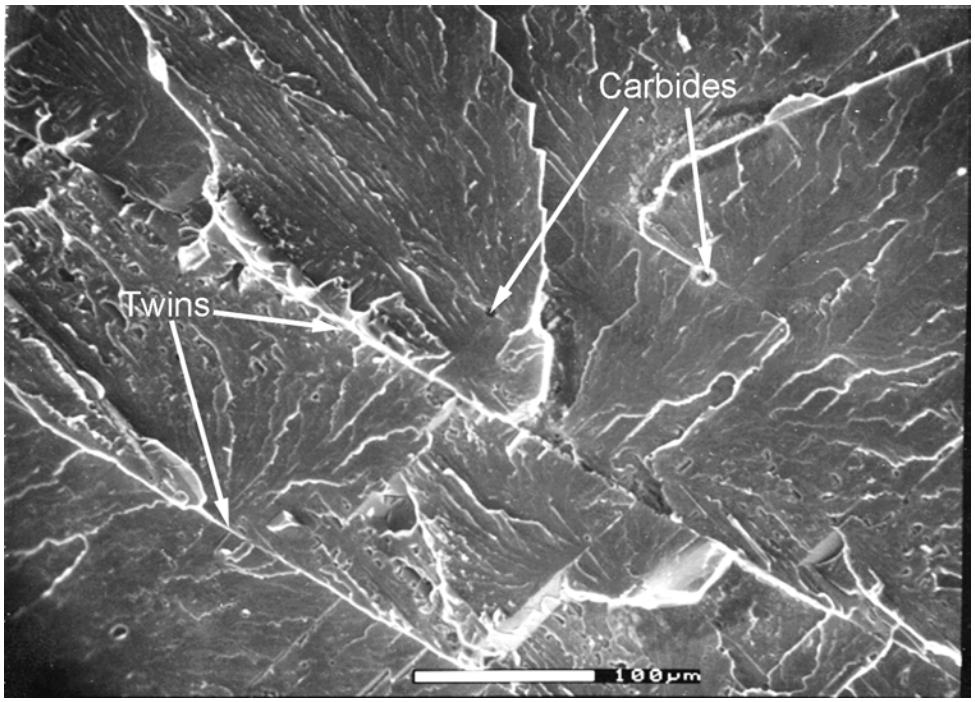

Fig.5 A SEM micrograph of the fracture surface in grain *A* showing repeated arrest and reinitiation of the cleavage crack by deformation twins.

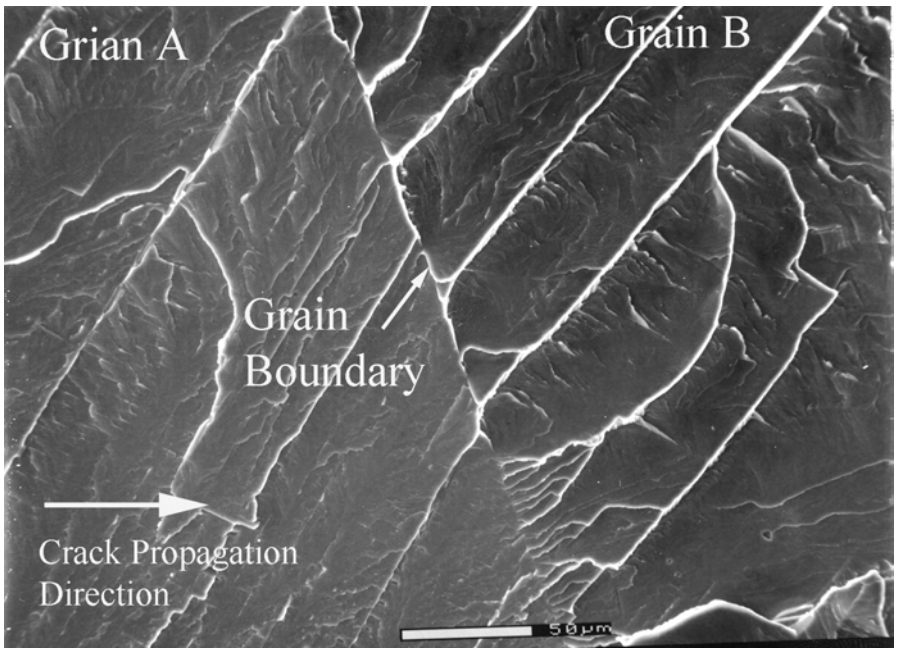

(a)

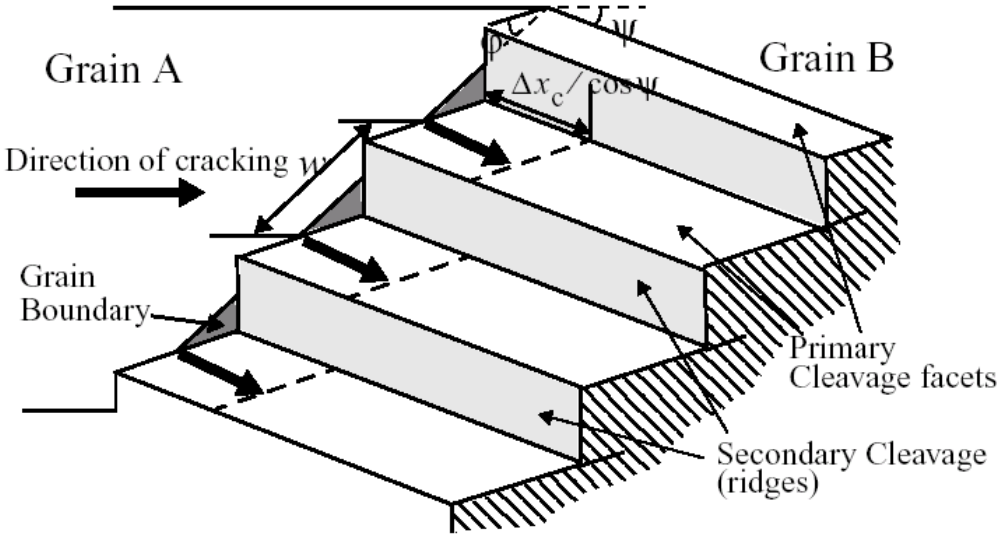

(b)

Fig.6 (a) A SEM micrograph showing a regular mode of break-through of the grain boundary from grain *A* to grain *B* with entry of the cleavage crack across the grain boundary at points a distance *w* apart and spreading out in grain *B* on a tiered stair-case-like mode (in bicrystal 10); (b) A sketch depicting the process of the cleavage crack penetrating from grain *A* into grain *B* in a regular mode, as shown in Fig.6a.

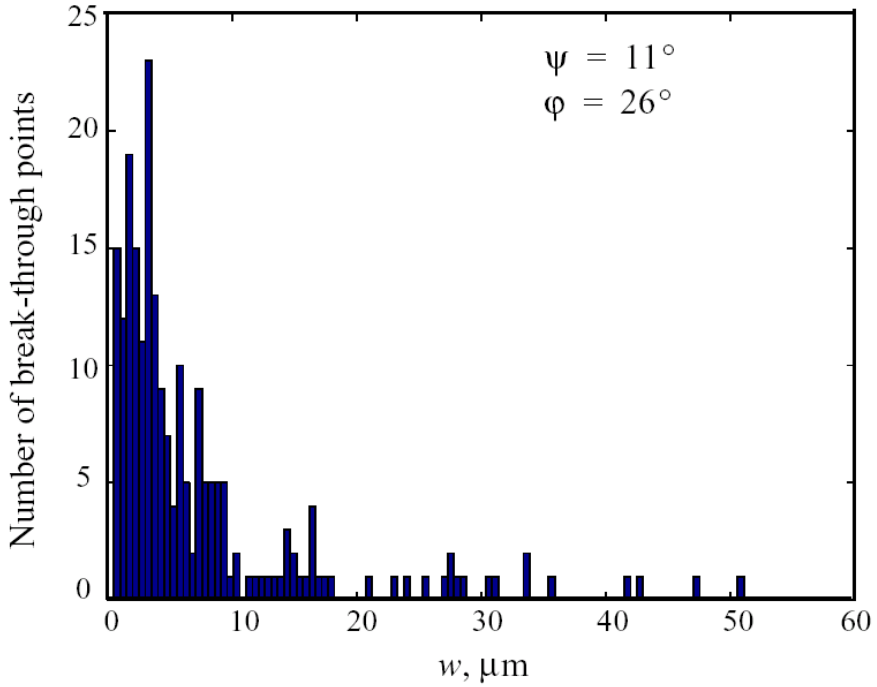

Fig. 7 The measured frequency distribution of distance w at a grain boundary with intermediate misorientation angles $\psi = 11^{o}$ and $\varphi = 26^{o}$ (in bicrystal 14). Other distributions for grain boundaries with smaller and larger misorientations give similar results.

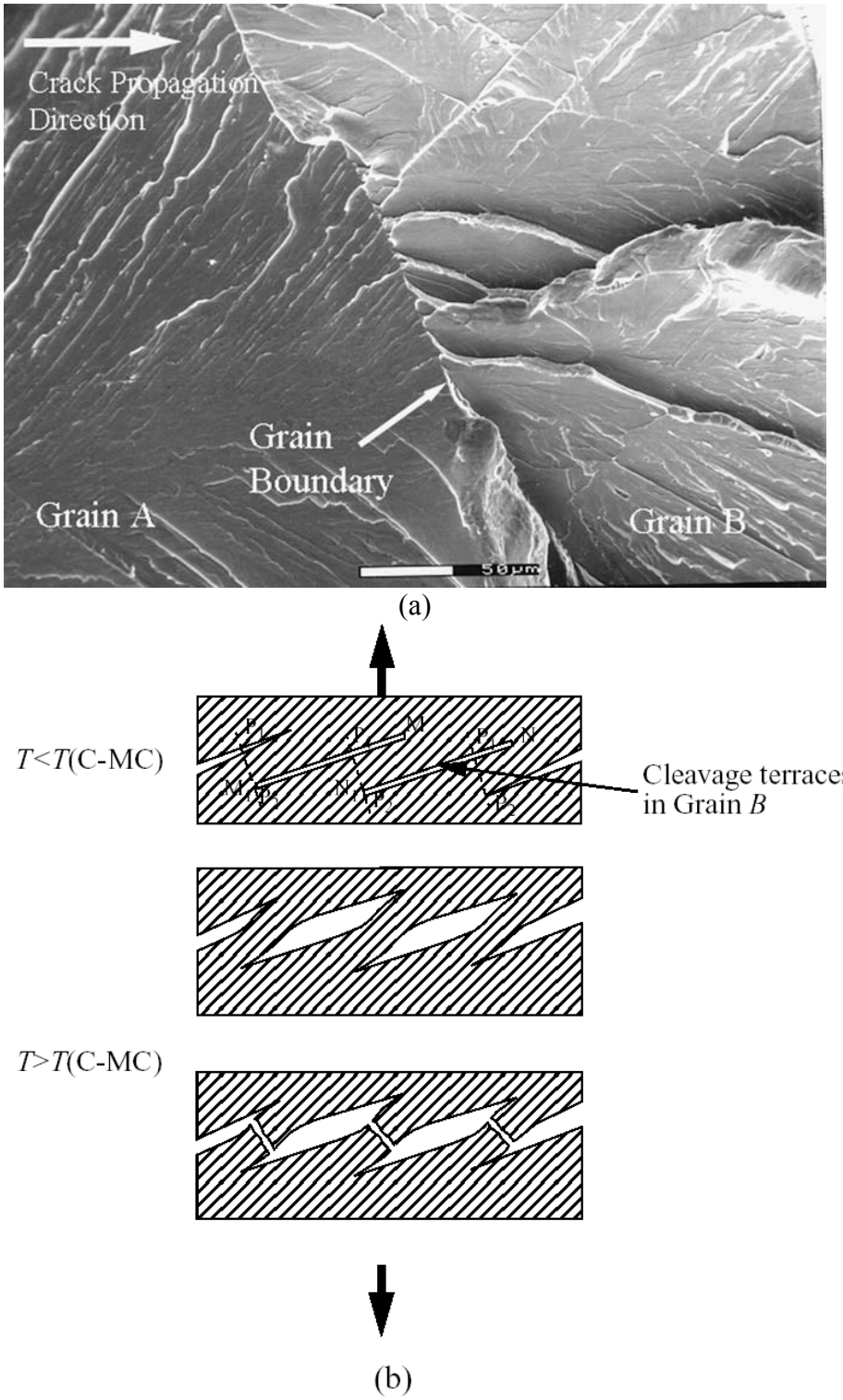

Fig. 8 (a) A SEM micrograph showing break-through across a grain boundary above the cleavage to mixed-cleavage transition; (b) cartoon depicting the nature of additional plastic dissipation by sigmoidal plastic bending and rupture of ligaments.

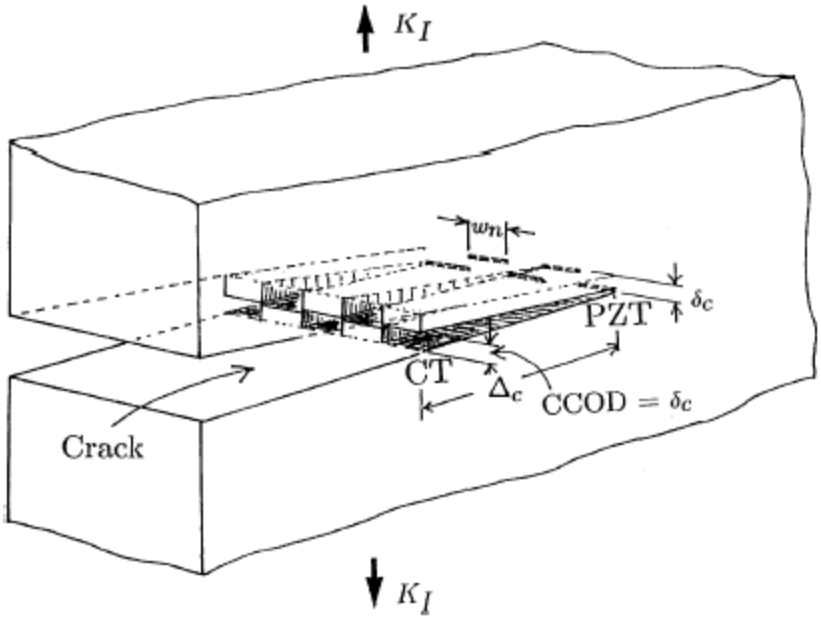

(a)

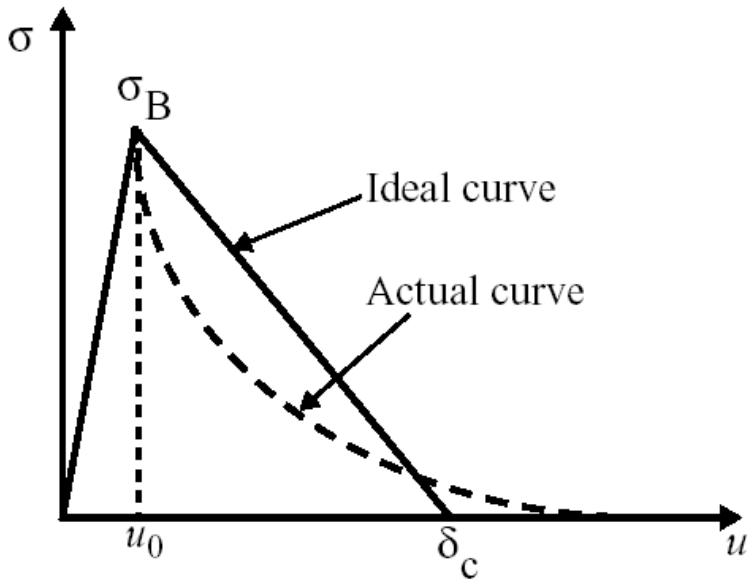

(b)

Fig. 9 (a) Propagation of a fragmented cleavage crack in grain *A* showing the nature of the plastic dissipation by plastic shear work in the bridging of cleavage strips; (b) The assumed tension/separation profile acting in a process zone of extent Δ_c.